Supporting Information

Li-Byarlay et al. 10.1073/pnas.1310735110

SI Materials and Methods

Image Processing. Treated and control bees were carefully paired. The fluorescent intensity of small interference RNA (siRNA) and nanoparticles (NPs) was measured by Axiovision software via the Measure ⇒ Interactive Measurement ⇒ Start Measurement function. All image data were saved in AxioVision ZVI format. Green channel (NP) and red channel (siRNA) signals were obtained separately and also compared with the background signals to ensure the baseline. A t test was used to assess statistical significance: control ($n = 10$) and *dnmt3* knockdown (KD; $n = 7$). All of the parameters for confocal setting were the same across all samples, including control and treatment bees.

RNA Isolation and Quantitative PCR. RNA was extracted from the fat bodies of each individual bee with the RNeasy kit according to the manufacturer's instructions (Qiagen). Knockdown of *dnmt3* was confirmed by quantitative PCR (qPCR) performed as previously described (1). We selected individuals showing typical KD for RNA sequencing (RNAseq). Primers designed for qPCR experiments and validations of alternative splicing (AS) are listed in Table S4. Sample sizes were 10 treated and 10 control individuals. Primers were designed to cross splice junction-spanning regions of the gene. Genomic DNA was also examined for each primer pair.

RNAseq. Of the 1,190 unexpressed genes, 762 are single-exon genes; only 389 unexpressed genes were annotated in a previous and more conservative annotation OGS v2.0. Read number for each sample is as follows—control sample: 1, 30,689,062 reads (×2); 2, 28,092,866 reads (×2); 3, 27,851,575 reads (×2); 4, 35,186,360 reads (×2); 5, 29,145,865 reads (×2); 6, 28,622,027 reads (×2); *dnmt3* KD sample: 1, 22,658,937 reads (×2); 2, 36,595,658 reads (×2); 3, 29,284,924 reads (×2); 4, 33,208,262 reads (×2); 5, 31,488,264 reads (×2); 6, 34,883,306 reads (×2).

Differential Expression Analysis. TrueSight assigns a probability score to each of the predicted splice junctions for each gene, which indicates their reliability based on coding potentials and RNAseq mapping quality. We used all splice junctions with a TrueSight score >0.5 (on a scale from 0 to 1) to refine the honey bee gene annotation available at the time of this study (Official Gene Set v3.2). A total of 4,274 (5.05% increase) new exons and 20,473 (29.5% increase) new splice junctions were added to OGS v3.2 to improve our analysis. Because the new junctions might originate from AS (alternative exon boundary) and lead to alternative boundaries for a single exon, we extended the original exon boundaries to the most remote junctions on that exon and built a nonredundant exon model for each gene. BEDTools was used to calculate the read coverage of the nonredundant exon models based on TrueSight mapping results (in binary alignment/map format). The sum of read numbers on all exons of a gene represents the digital gene expression value. The SAM (2) permutation test was used to test for differential expression; 2,613 genes (1,357 up-regulated and 1,256 down-regulated) were determined to be differentially expressed [false discovery rate (FDR) = 0.01, $n = 6$ treated and 6 control bees].

Analysis of Alternative Splicing. AS was annotated with the same procedure described in ref. 3. Results for the four subtypes of AS [intron retention (IR), exon skipping (ES), alternative exon boundary (AEB), and alternative terminal exon (ATE)] are summarized in Table 1.

Differential Alternative Splicing. We used two sources of information to test the significance of differentially spliced genes (DSGs). The first approach was to use RNAseq coverage, using both fully mapped reads and junction-spanning reads from RNA-seq; the second approach was to focus on splice junctions, by counting the number of junction-spanning reads from RNA-seq reads on splice junctions involved in AS.

Testing DSG Using Exon/Intron Coverage (P_{cov}). DSGs including IR, ES, and ATE were detected based on the coverage ratio changes for the retaining introns, skipped exons, and alternative terminal exons, respectively. An unpaired t test was used to calculate the P value, P_{cov}, from coverage ratios. Because AEBs often differ by just a few base pairs, exon coverage information cannot be generally applied to AEB differential splicing; only splice junction mapping counts were used to calculate P_{count} (see below).

Testing DSG Using Alternative Splice Junction Mapping Counts (P_{count}). The change in the number of RNA-seq reads mapped onto alternative splice junctions was used to calculate another statistic to test DSG in ES, AEB, and ATE. Fisher's exact test was used to calculate the P value, P_{count}, from alternative splice junction mapping counts. Because IR is for intron expression rather than alternative splice junction, differential IR cannot be tested with junction mappings; only coverage information was used to get P_{cov} (see above).

P_{cov} is the final P value for testing IR and P_{count} is the final P value for testing AEB. For ES and ATE, both statistical testing metrics were applied, and we used Fisher's combined probability test to obtain the final P values: $\chi^2 = -2\log(P_{cov}) - 2\log(P_{count})$. P values were adjusted for multiple hypotheses testing by using a Benjamini-Hochberg FDR criterion. The detailed testing procedure is described below for each subtype of AS.

$$N(x\sim y) = \text{number of reads mapped onto junction } x\sim y$$

$$\text{Cov}(x\sim y) = \frac{\sum_{i=x}^{y}\text{number of reads mapped onto } i}{y-x}.$$

Differential intron retention test. For a retained intron with coordinates $p \sim q$ and two adjacent exons $a \sim p$, $q \sim d$, its inclusion ratio was calculated as follows:

$$\text{IR inclusion ratio} = \frac{2 * Cov(p\sim q)}{Cov(a\sim p) + Cov(q\sim d)}.$$

Unpaired t tests were used on IR inclusion ratios to get P_{cov}, and on that basis, 27 IRs were determined to be DSG (FDR = 0.1; Benjamini-Hochberg). In the example of IR in Fig. 3, control is calculated as $2 \times 40.6/(168.6 + 159.1) \approx 0.25$; *dnmt3* KD is calculated as $2 \times 28.8/(196.1 + 201.9) \approx 0.14$.

Differential exon skipping test. We applied both metrics to measure changes of ES by *dnmt3* KD. For an ES with coordinates $p \sim q$ and two adjacent constitutive exons $a \sim b$, $c \sim d$, the ES skipping ratio was calculated as follows:

$$\text{ES skipping ratio} = \frac{Cov(a\sim b) + Cov(c\sim d) - 2 * Cov(p\sim q)}{Cov(a\sim b) + Cov(c\sim d)}.$$

P_{cov} was calculated using an unpaired t test.

The second method used the number of junction mapping reads. The ES-containing isoform was represented by $I_c = \text{int}\left(\frac{N(b\sim p)+\ N(q\sim c)}{2}\right)$ and the CE-skipping isoform by $I_s = N(b\sim c)$.

For Table 2, we chose 192 differential exon skipping (DES) events together with their flanking 200-bp intronic regions and computed the average change in methylation for each region in *dnmt3* KD vs. control bees. There were 72 DESs overlapping with methylated cytosine-phosphate-guanine (mCpG) sites. Using these 72 DESs, there was a significant relationship between *dnmt3* KD, DNA methylation, and DES; decreased methylation (due to *dnmt3* knockdown) was associated with increased exon skipping (P = 0.019, two-tailed Fisher's exact test). The same analysis was performed for differential intron retention (DIR). Using 15 DIRs, there was also a strong trend with decreased methylation associated with less intron retention (P = 0.044, two-tailed Fisher's exact test).

Although per-sample RNA-seq coverage is decent in our data, minor isoforms generated from AS might still have low sequencing coverage. Therefore, directly comparing the splice junction (SJ) counting ratios across samples would be misleading. We summed all control and *dnmt3* treatment mapping numbers, respectively, performed the Fisher's exact test on the 2 × 2 table $\left[\sum_{i=1}^{6} I_c(i) : \sum_{i=1}^{6} I_s(i);\ \sum_{j=1}^{6} I_c(j) : \sum_{j=1}^{6} I_s(j)\right]$, and calculated P_{count}.

Fisher's combined probability test was performed based on coverage and junction read counts, and the final P value calculated from $\chi^2 = -2\log(P_{cov}) - 2\log(P_{count})$, with four degrees of freedom. A total of 192 ESs were selected as DSGs (0.01 FDR; Benjamini-Hochberg). In the example of ES in Fig. 3, control is calculated as 90/(25 + 46) × 2 ≈ 2.5; *dnmt3* KD is calculated as 197/(40 + 62) × 2 ≈ 3.9.

Differential AEB test. Because the majority of AEBs are of a few base pairs difference, the coverage information could not be applied to differentiate the use of AEBs. Instead, we used RNA-seq read counts on alternative splice junctions in testing differential AEB, as follows.

Let us assume that for three continuous exons ($a \sim b$, $p \sim q$, $c \sim d$), exon $p \sim q$ has alternative splice site p'.

The number of isoforms containing junction $b \sim p$ is $I_p = N(b \sim p)$, and the number of isoforms containing junction $b \sim p'$ is $I_{p'} = N(b \sim p')$. The same Fisher's exact test strategy as used in the differential ES test was applied here in AEB testing.

We determined 141 ATEs to be significantly differentially spliced after *dnmt3* KD, at 0.01 FDR (Benjamini-Hochberg). In the example of AEB in Fig. 3, control is calculated as 121/37 ≈ 3.3; *dnmt3* KD is calculated as 110/10 = 11.

Differential ATE test. Assume that we have a constitutive exon ($a \sim b$), and two ATEs ($c \sim d$, $e \sim f$).

Using the coverage information, ATE splicing ratio was calculated as follows:

$$\text{ATE splicing ratio} = \frac{Cov(c\sim d)}{Cov(c\sim d) + Cov(e\sim f)}.$$

P_{cov} was calculated using an unpaired t test.

The number of isoforms containing junction $b \sim c$ is $I_c = N(b \sim c)$, and the number of isoforms containing junction $b \sim e$ is $I_e = N(b \sim e)$. The same Fisher exact test strategy as used in ES was applied here in ATE testing to calculate P_{count}.

The final P value for ATE was calculated from $\chi^2 = -2\log(P_{cov}) - 2\log(P_{count})$, with four degrees of freedom. In total, 225 ATEs were determined to be DSGs (0.01 FDR; Benjamini-Hochberg). In the example of ATE in Fig. 3, control is calculated as 87/27 ≈ 3.2; *dnmt3* KD is calculated as 179/34 ≈ 5.3.

1. Alaux C, et al. (2009) Honey bee aggression supports a link between gene regulation and behavioral evolution. *Proc Natl Acad Sci USA* 106(36):15400–15405.
2. Li J, Tibshirani R (2011) Finding consistent patterns: A nonparametric approach for identifying differential expression in RNA-Seq data. *Stat Methods Med Res*, 10.1177/0962280211428386.
3. Li Y, et al. (2013) TrueSight: A new algorithm for splice junction detection using RNAseq. *Nucleic Acids Res* 41(4):e51.

ATGTTGTCCGAGGAAGGGAAATTATGGGTTTACTGGATCGGAGAAGCTCGTATATCATTA
TTGAACGAAAAGACGCAGATCGAACCGTTCTCGTGTAACCTCAAGGCTAGACTGACGCAG
AATTTAAACGTACCGCGAATTCGTGCCATTGACGCAACTATGCAGATGTTGCGCAAAAAA
TTGGGCGGTACTTTGACCAAGCCGTATTTCACGTGGATCGAAAGCAATTTCCCCAAAAAT
ATGATCGAAATGTTGGACGAAATCAAGTTTTATCCGTATCCGGTAAAGATGCAACAAAGA
TTGGACCATCTTAGGGAAAAAAAACGCAAAAGTAACGGAAAGATATTTATTGGATCAAAAA
CGGGAAAATCAAGAGAAAAAATTGGCTGAGAAGTCGAAAGATTCGCCGCAAAAAGTCAAC
GTAGATTTGACGCTTTTGCCGTTGAAAGAGCAGAAACCGGGAATTATAGCCTGGGCTAAA
ATTGCCGGGCACAATTGGTGGCCAGCGATGATTATCGATTATCGCGACTGTTGCATGCGA
GAACCGACGTTCGGTTGCCAATGGATCATGTGGTACGGCGACTACAAACTGTCGGAGGTG
CATCATCAATTGTTCTTGAGGTTCGACAAGGGGATGGAGAAAATGCGCGACTACACGAGC
AACACGAAGAAGCATATCTACCTCGTAGGAGTTCTCCAAGCCTCCAAGGATTATTGCTCC
CGTCTAGGATTCGATACCTCCAACTGGACTTTGGACGACGCTTTCGAATATTTTTCCAAG
CCTAATCATTACGATTACGCGTCGTCTGCGAACACTTGGAGGAGAGAAGACTCGGTCAAG
ATCTACGACAAGTACTCGGCCCGCATCGCGGAAAAATTGAACGAGCTGAAGGACAATCCG
AACGTGGACGACCAACGGGCCAACGATATAAACAACAGCGATGACCTGCGATCGGCGATA
AAAGGGGAAATCTCGTTCGACTCGTTGTGCCTCAAGTGCCTTCGAGTTTCCAACGACGAA
ATGGACATTCATCCGTTCTTCGAGGGATCTTTGTGCAAAGATTGTTCGGAACGATATAAA
CCCTGTATGTTCGTTTTCGGTAACGACTCCAAATGCTTTTATTGCACCGTGTGCGCCGCC
TCTGGGATGGTGATCATCTGCGACAAAGAAGATTGTCCAAGGGTTTACTGCACCGCCTGC
ATGAAACACCTCCTGTGCCCGACGACTTACGAGCAAGTGCTCCAGGAGGATCCTTGGGAA
TGCTTCCTCTGCAAGTCAAGATCTTTCACCACAGACACCATCGTCAGGCCTCGAGCTAAT
TGGAAGGACAAGATAATCAATATGTTCCGTACCAGTTGCGACTCGAATGTGGAACACCTG
GTTGCCAAGCATAATTCAGAGAAGAGAAAAATACGCGTTCTCTCCCTGTTCGACGGCCTT
GGCACAGGTTTGCTCGTACTTCTGAAACTGGGCTTCATCGTGGACGCGTATTACGCGAGC
GAGATAGACCAAGACGCGTTGATGGTTACCGCCTCGCACTTCGGCGACCGTATCCTCCAA
TTGGGCAACGTGAAGGACATCACGTGTAACACGATCAAAGAGATAGCTCCCATCGATCTT
CTGATCGGTGGATCGCCGTGCAACGATCTCAGCTTGGCCAATCCTGCCCGCCTCGGCCTC
CACGATCCCAGAGGAACGGGTGTACTGTTCTTCGAGTACCGTCGAATTCTGAAACTGGTG
AGGAAGCTTAATAACGAGCGGCATTTGTTCTGGTTGTACGAGAACGTCGCCTCGATGCCC
AGCGAGTACAGATTGGAGATCAACAAACATCTAGGACAGGAACCGGACGTGATAGACTCG
GCAGACTTCTCGCCCCAGCACAGATTGAGACTGTACTGGCACAACTTTCCCATAGAGCCA
CGTCTGTTATCGTCCCAAAGGGAGCAGGACGTGCAGGATATACTTACGCCGCATTGCCAA
CGTTACTCGTTGGTCAAAAAGATACGCACAGTCACTACGAAAGTGAACTCGTTGAAGCAA
GGTGATGGCAAACTTGCGTTGAAACCAATTTTGATGAAGGACGAAAGCGACTCGTTGTGG
ATAACAGAGCTGGAGGAAATATTCGGGTTCCCGCGTCATTACACGGACGTAAAGAATTTA
TCTGCGACGAAAAGGCAGAGGTTAATAGGTAAATCTTGGAGCGTGCAAACGTTGACAGCC
ATTTTCGAATCTCTTTGTCCCTTTTTCGAGCGCGATATCGTGGAAATCGAGGGATGA

Fig. S1. mRNA sequence of *dnmt3* (GB55485) and KD sites. The italicized and gray colored sequences are the siRNA target sites (exon 5, location starts at 413; ref. 1). The underlined and yellow colored sequences are the qPCR primers (exon 12, location of forward primer starts at 1,211, and reverse primer at 1,273).

1. Kucharski R, Maleszka J, Foret S, Maleszka R (2008) Nutritional control of reproductive status in honeybees via DNA methylation. *Science* 319(5871):1827–1830.

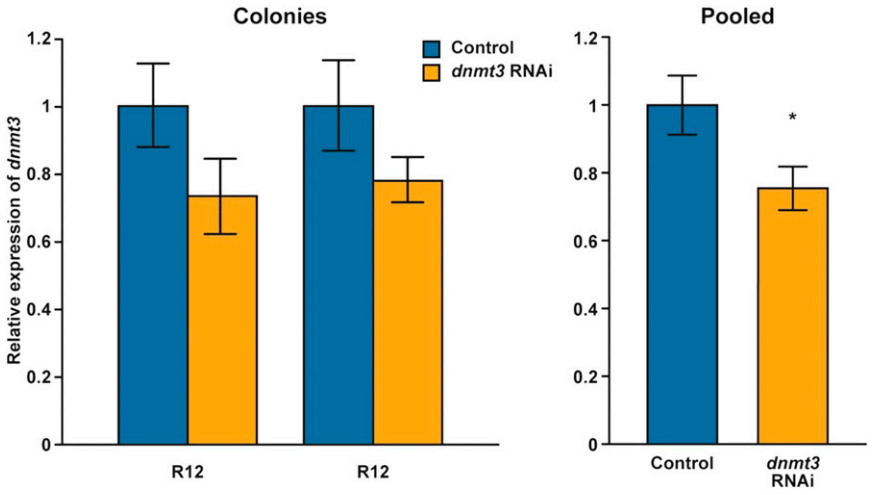

Fig. S2. KD effects on *dnmt3* mRNA expression by injecting *dnmt3* siRNA in the abdomen of honey bees (mean and SEM). Shown are two biological replicates ($n = 21$ and 22, P values based on two-tailed t-tests) and results from pooled data (mixed-model ANOVA, df = 40, $F = 6.18$, $^*P < 0.05$).

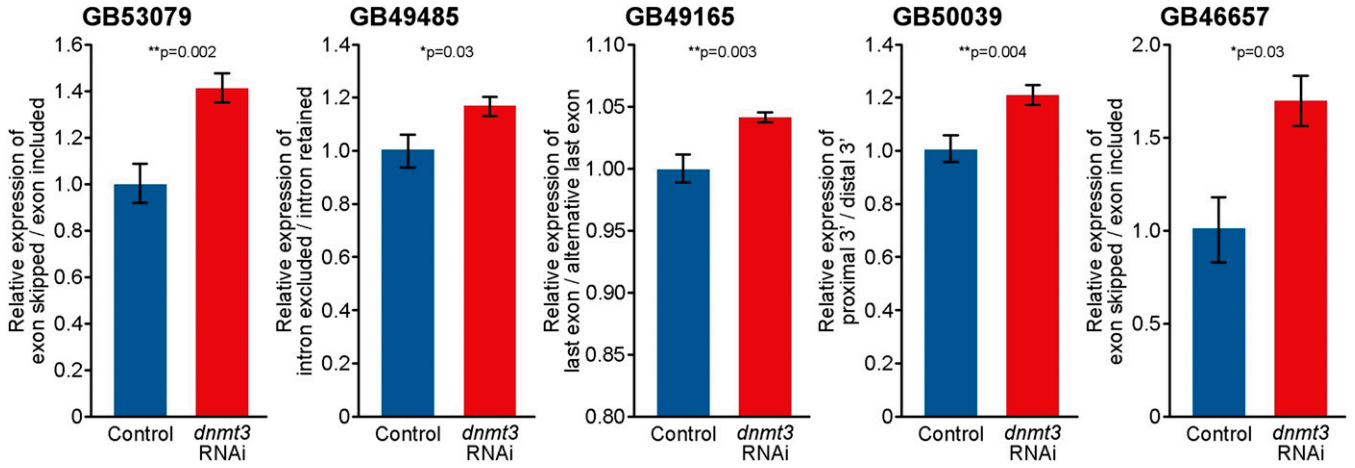

Fig. S3. Validation of *dnmt3* RNAi-associated alternative splicing. To validate the splicing results, gene candidates for each type of AS event were selected for qPCR analysis. ES was validated with *GB53079* (motile sperm domain-containing protein 1-like) and *GB46657* (galactokinase-like); IR with *GB49485* (probable prolyl-tRNA synthetase, mitochondrial-like); ATE with gene *GB49165* (protein RER1-like); and AEB with gene *GB50039* (methionyl-tRNA synthetase). Control: $n \geq 10$; *dnmt3* KD: $n \geq 10$. Mean relative expression levels, SEM, and *P* values are displayed. Data analyzed with two-tailed *t* tests.

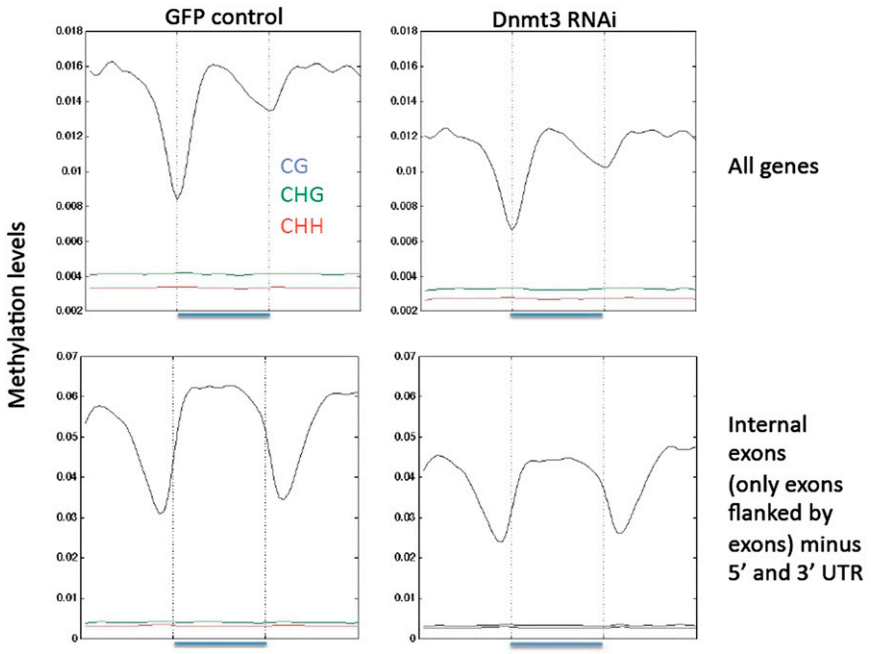

Fig. S4. Methylation levels for control and *dnmt3* KD bees ($n = 1$ pooled sample for each). Top two graphs show all genes; bottom two graphs show internal exons only. C stands for cytosine, G stands for guanine, H stands for adenine (A), thymine (T), or cytosine (C). The colors blue, green, and red represent CG, CHG, and CHH sequences, respectively. The middle section (underlined blue) of each graph represents the whole gene or just the internal exon.

Table S1. Gene Ontology (biological process) analysis of genes that were differentially expressed between control bees and *dnmt3* KD bees (Benjamini cutoff: <0.01)

Term	Count	Percentage	*P* value	Fold enrichment	Benjamini
GO:0042254~ribosome biogenesis	44	2.31	2.91E−20	4.32	7.21E−17
GO:0022613~ribonucleoprotein complex biogenesis	51	2.68	4.23E−17	3.41	5.24E−14
GO:0034660~ncRNA metabolic process	61	3.21	9.67E−16	2.88	8.25E−13
GO:0006396~RNA processing	102	5.36	1.25E−13	2.06	7.74E−11
GO:0034470~ncRNA processing	43	2.26	1.27E−11	2.94	6.30E−09
GO:0006364~rRNA processing	25	1.31	2.60E−10	3.93	1.07E−07
GO:0006413~translational initiation	30	1.58	2.65E−10	3.43	9.37E−08
GO:0016072~rRNA metabolic process	25	1.31	5.33E−10	3.83	1.65E−07
GO:0046907~intracellular transport	90	4.73	7.16E−09	1.81	1.97E−06
GO:0030163~protein catabolic process	65	3.42	7.51E−09	2.04	1.86E−06
GO:0019941~modification-dependent protein catabolic process	57	3.00	1.66E−08	2.12	3.75E−06
GO:0043632~modification-dependent macromolecule catabolic process	57	3.00	2.11E−08	2.11	4.35E−06
GO:0044257~cellular protein catabolic process	60	3.15	2.15E−08	2.06	4.09E−06
GO:0051603~proteolysis involved in cellular protein catabolic process	60	3.15	2.15E−08	2.06	4.09E−06
GO:0034621~cellular macromolecular complex subunit organization	64	3.36	3.65E−08	1.98	6.45E−06
GO:0034622~cellular macromolecular complex assembly	55	2.89	4.84E−08	2.10	7.99E−06
GO:0043933~macromolecular complex subunit organization	80	4.21	8.81E−08	1.79	1.36E−05
GO:0006399~tRNA metabolic process	37	1.95	1.08E−07	2.48	1.57E−05
GO:0065003~macromolecular complex assembly	72	3.79	1.31E−07	1.84	1.81E−05
GO:0044265~cellular macromolecule catabolic process	67	3.52	1.89E−07	1.87	2.47E−05
GO:0007010~cytoskeleton organization	116	6.10	2.50E−07	1.57	3.10E−05
GO:0045184~establishment of protein localization	79	4.15	3.59E−07	1.74	4.23E−05
GO:0015031~protein transport	77	4.05	5.33E−07	1.74	6.00E−05
GO:0008104~protein localization	100	5.26	6.45E−07	1.60	6.95E−05
GO:0009057~macromolecule catabolic process	76	4.00	9.53E−07	1.73	9.83E−05
GO:0007017~microtubule-based process	102	5.36	1.06E−06	1.58	1.05E−04
GO:0051169~nuclear transport	29	1.52	1.95E−06	2.53	1.86E−04
GO:0006913~nucleocytoplasmic transport	29	1.52	1.95E−06	2.53	1.86E−04
GO:0006457~protein folding	39	2.05	3.61E−06	2.13	3.31E−04
GO:0060341~regulation of cellular localization	27	1.42	6.51E−06	2.50	5.75E−04
GO:0000226~microtubule cytoskeleton organization	77	4.05	9.17E−06	1.63	7.83E−04
GO:0006886~intracellular protein transport	51	2.68	1.09E−05	1.84	8.99E−04
GO:0034613~cellular protein localization	52	2.73	1.16E−05	1.83	9.25E−04
GO:0016192~vesicle-mediated transport	95	4.99	1.17E−05	1.53	9.05E−04
GO:0006605~protein targeting	36	1.89	1.76E−05	2.08	1.32E−03
GO:0006325~chromatin organization	49	2.58	2.70E−05	1.81	1.96E−03
GO:0016568~chromatin modification	36	1.89	3.37E−05	2.02	2.38E−03
GO:0007051~spindle organization	60	3.15	3.88E−05	1.68	2.66E−03
GO:0006612~protein targeting to membrane	15	0.79	4.45E−05	3.25	2.98E−03
GO:0007052~mitotic spindle organization	53	2.79	5.93E−05	1.72	3.86E−03
GO:0044087~regulation of cellular component biogenesis	28	1.47	5.99E−05	2.20	3.80E−03
GO:0016044~membrane organization	78	4.10	6.32E−05	1.54	3.90E−03
GO:0007242~intracellular signaling cascade	73	3.84	9.41E−05	1.55	5.67E−03
GO:0009451~RNA modification	17	0.89	1.02E−04	2.81	6.01E−03
GO:0000022~mitotic spindle elongation	27	1.42	1.03E−04	2.18	5.93E−03
GO:0006897~endocytosis	65	3.42	1.13E−04	1.58	6.33E−03
GO:0010324~membrane invagination	65	3.42	1.13E−04	1.58	6.33E−03
GO:0006338~chromatin remodeling	19	1.00	1.20E−04	2.60	6.59E−03
GO:0043623~cellular protein complex assembly	28	1.47	1.22E−04	2.12	6.57E−03
GO:0070727~cellular macromolecule localization	62	3.26	1.28E−04	1.60	6.75E−03
GO:0051231~spindle elongation	27	1.42	1.31E−04	2.15	6.74E−03
GO:0006461~protein complex assembly	46	2.42	1.60E−04	1.73	8.06E−03
GO:0070271~protein complex biogenesis	46	2.42	1.60E−04	1.73	8.06E−03
GO:0007317~regulation of pole plasm oskar mRNA localization	13	0.68	1.69E−04	3.27	8.33E−03
GO:0006909~phagocytosis	52	2.73	1.81E−04	1.66	8.73E−03

Table S2. Effects of *dnmt3* KD on expression and methylation of genes known to encode splicing factors (based on orthology to *Drosophila melanogaster*)

OGS3.2 Gene name	Up-regulated (Q value)	Down-regulated (Q value)	Fold change	Fold change: gene body methylation	Fold change: promoter	Fly ortholog	Gene function
GB51710		0.61	0.81	1.22	0.49	FBgn0001942	Eukaryotic initiation factor 4A-like
GB50757		0.53	0.85	0.66	0.71	FBgn0022987	KH domain-containing, RNA-binding, signal transduction-associated protein 3–like [*Apis mellifera*]
GB55439		0.49	0.89	1.04	0.00	FBgn0010220	DEAD box protein 45A ortholog
GB42714	0.68		1.11	0.99	0.63	FBgn0086683	Splicing factor 45-like
GB49296	0.85		1.11	0.80	1.96	FBgn0030974	U2AF_lg; U2 snRNP auxilliary factor, large subunit, splicing factor
GB48312	0.25		1.13	0.99	0.94	FBgn0037220	Pre-mRNA-splicing factor RBM22-like
GB48261	0.06		1.15			FBpp0084626	116-kDa U5 small nuclear ribonucleoprotein component–like
GB50695	0.56		1.17	0.98	0.98	FBgn0086444	Probable pre-mRNA-splicing factor ATP-dependent RNA helicase mog-4–like
GB44439	0.09		1.18	1.10	1.13	FBgn0037573	Eukaryotic initiation factor 4A-III–like
GB50078	0.62		1.20	0.67	0.75	FBgn0015331	ATP-dependent RNA helicase activity
GB51256	0.09		1.25	0.53	0.98	FBgn0036314	PRP11; Splicing factor 3a, subunit 2 [RNA processing and modification]
GB42720	0.09		1.36	1.12	1.29	FBgn0014189	Helicase at 25E ortholog
GB42279	0.21		1.38	0.97	0.00	Null	DEADc; DEAD-box helicases; a diverse family of proteins involved in ATP-dependent RNA unwinding, needed in a variety of cellular processes including splicing, ribosome biogenesis and RNA degradation
GB40538	0.09		1.67	1.40	0.91	FBgn0021995	Probable ATP-dependent RNA helicase DDX27-like
GB50605	0.09		1.70	0.76	0.00	FBgn0038609	Putative pre-mRNA–splicing factor ATP-dependent RNA helicase DHX15-like
GB44884	0.21		1.89	0.98	1.59	FBgn0035162	Splicing factor 3b, subunit 3, 130 kDa

Gene list obtained from the National Center for Biotechnology Information (NCBI) database.

Table S3. siRNA sequence designed for RNA interference (ref. 1)

siRNA	Sense	Antisense
EGFP-S1 DS positive control duplex	ACCCUGAAGUUCAUCUGCACCACCG	CGGUGCAGAUGAACUUCAGCCUCA
dnmt3	GUCAACGUAGAUUUGACGCdTdT	GCGUCAAAUCUACGUUGACdTdT

1. Kucharski R, Maleszka J, Foret S, Maleszka R (2008) Nutritional control of reproductive status in honeybees via DNA methylation. *Science* 319(5871):1827–1830.

Table S4. Primers used for qPCR experiments

Primer names	Forward	Reverse
Eif3-S8	TGA GTG TCT GCT ATG GAT TGC AA	TCG CGG CTC GTG GTA AA
GAPDH	ACT GGT ATG GCC TTC CGT GTA C	TGC CAA GTC TAA CTG TTA AGT CAA CA
dnmt3	TCC TGT GCC CGA CGA CTT A	TGC AGA GGA AGC ATT CCC A
GB53079 exon included	GTC CAG CTA TAC AAA TGA TTC CAG C	ATG CTA TGG ATA AAG GAG GAA CAA A
GB53079 exon skipped	GTC CAG CTA TAC AAA TGA TTC CAG C	CAA AAT AAA GCA ATT GAT AGA GGA ACA A
GB50039 ctrl-186–495	TCT TCC TGT TTT TCT TTT TTT TTT TGT AAC	TTT ACA ACG TGT CAA AAA TCA AGA GA
GB50039 -178–495	AAA TGT GAT TTT GCT TCA CTT TGA TAA A	ACG TGT CAA AAA TCA AGA GAA GTT ACA A
GB49165 -9476082–2735	TTC CTT AGG TTA GCG CCA AGA T	CTC ATG GAA AAC CAA AGT ACC AGA
GB49165 -9480053–2735	CCA TCA CCA AAT TTC CAC GG	CTC ATG GAA AAC CAA AGT ACC AGA
GB53833 -9158642–8319	TGA ACA TCA AGA CGA AGT GGA TG	CGT CTA TAC GCT TGG TCA GCC T
GB53833 -9191360–8319	AAA TCA AGA GCA TCG TGA TCG AG	CGT CTA TAC GCT TGG TCA GCC T
GB49485 E1	TGG CCA AAA AAT TTA GCA CCA	TTT TCT TCT TTG CTT CCT GCC T
GB49485 E2	GAA GAA TTA AGA TGG CCA AAA AAT TTA	ATA CCC TTT TAT ATA TTA CCT TTG GTG GT
GB46657 exon included	TCG TGT GAA TTT AAT CGG AGA ACA	GTA ACC ATG GGC AAT GCC A
GB46657 exon skipped	TGT ATG TGC ACC CGG TCG	GCA TTA AAA GGT GGC ACA TCA C